RSC Advances

ROYAL SOCIETY OF CHEMISTRY

www.rsc.org/advances

Cite this: DOI: 10.1039/c0xx00000x

www.rsc.org/xxxxxx

ARTICLE TYPE

Fabrication of Cu-Ag bimetal nanotube-based copper silicates for enhancement of antibacterial activities

Weijun Fang, *[a, #] chaofa Xu[b, #] Jun Zheng,*[c] Guangjun Chen[a] and Kong Jiang[a]

Received (in XXX, XXX) Xth XXXXXXXXX 20XX, Accepted Xth XXXXXXXXX 20XX

DOI: 10.1039/b000000x

A novel Cu-Ag bimetal antibacterial system was reported. In this Cu-Ag bimetal system, copper silicate nanotubes (CSNTs) and copper silicate nanotube-assembled hollow nanospheres (CSNAHSs) with high BET surface area, unique hollow structure and strong antibacterial activity, were adopted as a carrier for loading silver ions to fabricate the copper-silver bimetal antibacterial agents (designated as Ag^+/CSNTs and Ag^+/CSNAHSs). Additionally, the antibacterial activity of Ag^+/CSNTs and Ag^+/CSNAHSs was investigated against Gram-negative bacteria (*Escherichia coli* BL21 and *Escherichia coli* JM109) and Gram-positive bacteria (*Staphylococcus aureus* and *Bacillus subtilis*). The results demonstrated that both silver-loaded copper silicates were highly effective against the four types of bacterial strains, and the Ag^+/CSNAHSs showed a stronger antibacterial ability than Ag^+/CSNTs due to their more silver loading contents. More importantly, a synergistic effect of copper ions and silver ions on the inhibition of the bacterial growth was observed in our bimetal antibacterial system.

1. Introduction

Mesoporous silica materials containing metallic ions have been extensively studied because of their unique physicochemical properties and potential applications in catalysis, batteries, sensors, separations, biomedicine, and so on.[1-6] Such properties mainly depend on the introduced metal species. Many metal ions embedded in mesoporous silica materials have been reported, [7-15] such as Fe^{3+}, Ni^{2+}, Zn^{2+}, Cu^{2+}, Mg^{2+} and Nb^{5+}. Among these metal ions, copper ion has attracted great attention owing to its unique catalytic ability and good antibacterial activity.[16-23]

Recently, various approaches have been developed to synthesize nanotube-based mesoporous copper silicates,[24-27] which demonstrated high adsorption capabilities and effective catalytic activities due to their high surface area, stability and sole catalytic active site. Most researches were focused on studying the catalytic activities of these copper silicates. Unfortunately, investigations on their biological properties are still scarce, as tubular structures could offer some interesting advantages over spherical particles for some biological applications, such as drug delivery, gene transfection and enzyme immobilization. [28-31]

In this study, we report a facile route to prepare copper silicate nanotubes (CSNTs) and nanotube-assembled hollow nanospheres (CSNAHSs). Furthermore, the as-prepared copper silicates are adopted as a carrier for loading silver ions to fabricate the Cu-Ag bimetal antibacterial agents (designated as Ag^+/CSNTs and Ag^+/CSNAHSs). Subsequently, four types of bacteria are selected to investigate and compare the antibacterial activities of the two kinds of Cu-Ag bimetal silicates. Three important features are associated with our bimetal antibacterial system: 1) Compared to other metal ions carriers, the nanotube-based copper silicates are used as the carrier which show antibacterial effects because of the presence of copper ions possessing the antibacterial activities. 2) Microorganisms have different tolerance against different kinds of antimicrobial materials. Herein, the as-prepared Cu-Ag bimetal silicates could exhibit higher antibacterial activities and wider antibacterial spectra than single ones.[32-36] 3) The CSNAHSs, have a unique hollow structure which offers effectively improved silver loading capacity. Based on these unique characteristics, the silver-loaded nanotube-based copper silicates are expected to be good candidates for antibacterial materials.

2. Experimental procedures

2.1 Materials

Tetraethoxysilane (TEOS) was purchased from Alfa Aesar. Copper nitrate ($Cu(NO_3)_2{\cdot}3H_2O$), ammonium aqueous solution ($NH_3{\cdot}H_2O$, 25-28%), silver nitrate ($AgNO_3$) and ammonium nitrate (NH_4NO_3) were purchased from Sinopharm Chemical Reagent Co. Ltd. (Shanghai, China). The other reagents were analytical grade and were used without any purification.

2.2 Synthesis of $sSiO_2$ nanoparticles

Solid SiO_2 ($sSiO_2$) were prepared using a modified Stöber method. Typically, 74 mL of ethanol, 3.15 mL of ammonium aqueous solution (~28%) and 10 mL of ultrapure water were mixed and further stirred for 1 h. The mixture was then heated up to 50℃, and 6 mL of TEOS was added. After the reaction with stirred for 6 h, $sSiO_2$ were obtained by centrifugation, washed with ethanol, and finally re-dispersed in 24 mL of water for subsequent use.

2.2 Synthesis of copper silicate nanotubes (CSNTs)

100.0 mg of $Cu(NO_3)_2 \cdot 3H_2O$, 0.6 g of NH_4NO_3, 0.5 mL of ammonium aqueous solution , 14.5 mL of ultrapure water, and 25.0 mg *s*SiO_2 nanoparticles were mixed and further stirred for 10 min. The mixture was then sealed in Teflon-lined stainless-steel autoclaves, and heated to 170℃ for 10 h. The final product was collected by centrifugation, and dried in air at 60℃ overnight.

2.3 Synthesis of copper silicate nanotube-assembled hollow nanospheres (CSNAHSs)

100.0 mg of $Cu(NO_3)_2 \cdot 3H_2O$, 0.9 mL of ammonium aqueous solution , 14.1 mL of ultrapure water, and 50.0 mg *s*SiO_2 nanoparticles were mixed and further stirred for 10 min. The mixture was then sealed in Teflon-lined stainless-steel autoclaves, and heated to 140℃ for 10 h. The product was collected by centrifugation, washed with ethanol, and dried in air at 60℃ overnight.

2.4 Synthesis of hollow mesoporous silica nanospheres (HMSHs)

The whole synthesis process of hollow mesoporous silica nanospheres (HMSHs) consists of two steps. Firstly, 8.2 mL of ethanol, 0.35 mL of ammonium aqueous solution and 1.1 mL of ultra-pure water were mixedand further stirred for 1 h. The mixture was then heated up to 50 ℃ and 0.67 mL of TEOS was added. After the reaction with stirring for 3 h, 2.5 mL of the mixture solution was added in 16.5 mL of ethanol/water mixture 1:2 (v/v), and then 7.5 mL of ethanol/water mixture 1:2 (v/v) containing 75 mg of CTAB was added. After 30 min of stirring, 120 μL of TEOS and 200 μL of ammonium aqueous solution were added to the above mixture. The mixture was allowed to react for 12 h at room temperature. The *s*SiO_2@CTAB/SiO_2 spheres were collected by centrifugation, and re-dispersed in 10 mL of water for subsequent use. Secondly, to transform *s*SiO_2@CTAB/SiO_2 spheres to HMSS spheres, 10 mL of the above solution containing *s*SiO_2@CTAB/SiO_2 spheres was mixed with 255 mg of Na_2CO_3. The reaction was stirred at 50 ℃ for 12 h, the HMSS spheres were harvested by centrifugation. The CTAB molecules were removed by ion exchange with NH_4NO_3.

2.5 Preparation of Ag^+/CSNTs, Ag+/CSNAHSs and Ag^+/HMSHs

$AgNO_3$ solution (2.0 mL) at a concentration of 2.5 mg/mL was mixed to 10 mg of CSNTs, CSNAHSs or HMSHs, and then the mixture was stirred in the dark at room temperature for 24 h. The Ag^+/CSNTs, Ag^+/CSNAHSs or Ag^+/HMSHs were obtained by centrifugation, washed with ultrapure water, and dried in an oven at room temperature.

2.6 Characterization

Transmission electron microscopy (TEM) studies were performed on a TECNAI F-30 high resolution transmission electron microscopy operating at 300 kV. Scanning electron microscopy (SEM) images were obtained on Hitachi S4800 scanning electron microscope with a field emission electron gun. The chemical state of silver in our samples was characterized by XPS (PHI Quantum 2000). The surface area and pore size distribution of the final products were determined by Surface Area and Porosity Analyzer (Micromeritics Instument Corp. ASAP2020).

2.7 Measurements of antibacterial properties of Ag^+/CSNTs and Ag^+/CSNAHSs by turbidimetric method

The antibacterial activities of the as-prepared Ag^+/CSNTs and Ag^+/CSNAHSs were valuated against *E. coli* BL21, *E. coli* JM109, *B. subtilis* and *S. aureus*. The inoculation of these kinds of bacteria were prepared by growing strains in LB (Luria-Bertani) liquid medium at 37 ℃ until a level of approximately 10^9 CFU/mL of bacteria was reached. Then 100 μL of 10^9 CFU/mL bacterial suspensions were added to 10 mL LB liquid medium containing different concentrations of Ag^+/CSNTs or Ag^+/CSNAHSs (0 μg/mL, 12.5 μg/mL, 25 μg/mL, 50 μg/mL and 100 μg/mL, respectively) and incubated at 37℃ with continuous agitation (180 rpm). The kinetics of bacterial growth was determined by measuring optical density (OD 600). Control experiments were also performed in the present of CSNTs or CSNAHSs.

2.8 Measurements of antibacterial properties of Ag^+/CSNTs and Ag^+/CSNAHSs by inhibition zone method

The antibacterial activities of the as-prepared Ag^+/CSNTs and Ag^+/CSNAHSs to *E. coli* BL21 and *S. aureus* were also investigated by inhibition zone method. Briefly, the sterile paper disks (9.0 mm) were impregnated with 20.0 μL of silver-loaded nanoparticles solution (2.5 mg/mL), and left to dry for 20 min at room temperature. Then, 150 μL of 10^7 CFU/mL bacterial suspensions were spread onto agar plates. The impregnated disks were placed on the agar plates and incubated at 37 ℃ for 14 h. After incubation, the diameter of the growth inhibition zones was measured. CSNTs and CSNAHSs (without Ag^+) were also used as the control experiments. All tests were done in triplicate.

2.9 Comparison of the antibacterial activities Ag^+/CSNAHSs, Ag^+/HMSHs and CSNAHSs

The inhibitory effect of the Ag^+/CSNAHSs, Ag^+/HMSHs and CSNAHSs were valuated against *E. coli* BL21. 100 mL of 10^9 CFU/mL bacterial suspension were added to 10 mL LB liquid medium containing different concentrations of the Ag^+/CSNAHSs, Ag^+/HMSHs or CSNAHSs, and incubated at 37℃ with continuous agitation (180rpm). After incubated for 8 h, the antibacterial efficacy was determined by measuring OD at 600 nm.

3. Results and Discussion

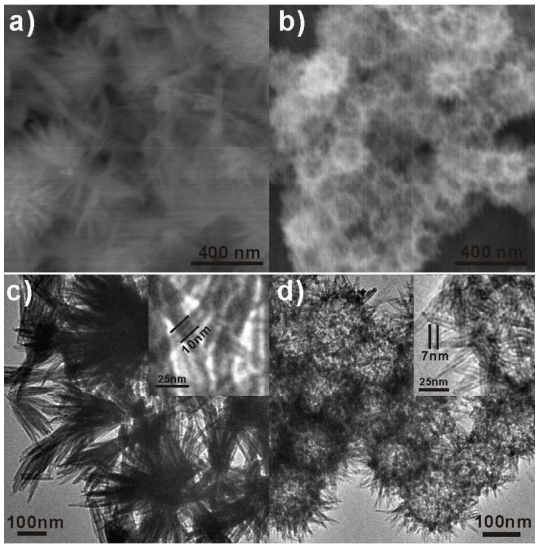

Figure 1. SEM images of (a) CSNTs and (b)CSNAHSs, TEM images of (c) CSNTs and (d) CSNAHSs.

Copper silicate nanotubes (CSNTs) and copper silicate nanotube-assembled hollow nanospheres (CSNAHSs) were successfully synthesized according to the modified method reported recently .[26] In our system, the morphology of the copper silicate could be easily tuned by controlling the reaction temperature and the amount of ammonia water using the Stöber SiO_2 spheres as silica source (see experimental sections for details). As shown in the scanning electron microscopy (SEM) images and the transmission electron microscopy (TEM) images (**Fig. 1**), CSNTs possess uniformly tubular shape with a mean length of ~ 270 nm (**Fig. 1a**) and a diameter of ~ 10 nm (**Fig. 1c** inset). Whereas, CSNAHSs (**Fig. 1b**) are consist of uniform hollow spheres with a diameter of ~ 210 nm. A closer look (inset of **Fig. 1d**) shows that the hollow spheres' shell is composed of copper silicate nanotubes, and the nanotubes have a narrow size distribution with a diameter of ~ 7 nm. N_2 adsorption/desorption analysis was also employed to investigate the porosity of CSNTs and CSNAHSs. Both samples show a typical type IV isotherm feature (**Fig. 2**). Barrett-Joyner-Halenda (BJH) calculations for the pore-size distribution center at 3.3 nm for CSNTs and 3.4 nm for CSNAHSs. The Brunauer-Emmett-Teller (BET) surface area is about 466.3 m^2/g for CSNTs and 490.5 m^2/g for CSNAHSs, and the total pore volume is 0.82 cm^3/g for CSNTs and 0.71 cm^3/g for CSNAHSs. These data indicate that CSNAHSs have a higher BET surface area than CSNTs.

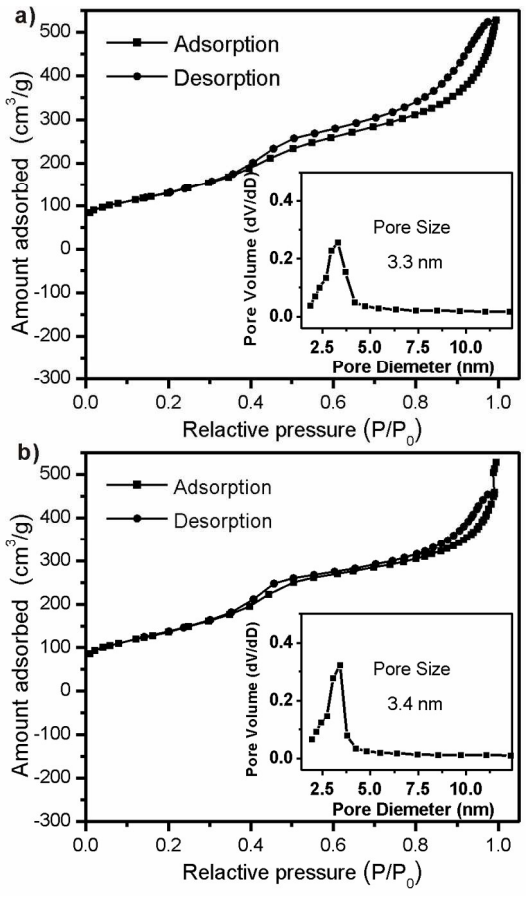

Figure 2. N_2 adsorption/desorption isotherms and the pore size distributions (inset) of (a) CSNTs and (b) CSNAHSs.

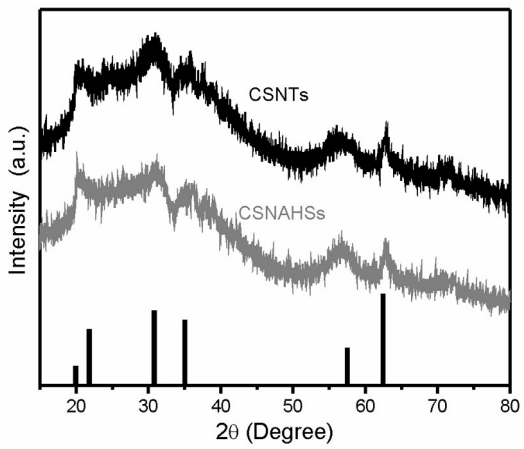

Figure 3. XRD patterns of CSNTs and CSNAHSs.

Fig. 3 shows the X-ray powder diffraction (XRD) patterns of CSNTs and CSNAHSs. It is clearly seen that the XRD patterns of the both samples appear almost the same, indicating that CSNTs and CSNAHSs have the same composition and phase. The main diffraction peaks centered at 19.99°, 22.03°, 30.8°, 35.03°, 57.44° and 62.61° can be indexed to copper silicate (JCPDS NO. 27-0188). The apparent broadening of these peaks suggests that the samples are composed of nanoscaled crystals.

It is well known that copper has been widely used in antibacterial fields due to its excellent antibacterial properties. Several reports have been demonstrated that copper-loaded composites exhibited both strong antibacterial effects and high antifungal activities.[37-40] So it is reasonable to believe that the as-prepared mesoporous copper silicates are ideal inorganic nanomaterials using as antibacterial agents. To further enhance their antibacterial activities and broadened their antibacterial spectra, Ag^+, a powerful antibacterial metal ion ,[41-46] was selected as an exchange ion to fabricate copper-silver bimetal nanoantibacterial agents. After loading with Ag^+, the final products were firstly studied by the energy-dispersive X-ray spectroscopy (EDX) and elemental mapping. As shown in **Fig. 4**, the main elements of both CSNTs and CSNAHSs are O, Cu and Si, and the content of these elements is nearly the same. However, the silver content in the Ag^+/CSNTs is 4.1% (W/W), which is lower than that in the Ag^+/CSNAHSs (6.8%, W/W). It maybe attributed to the unique hollow structure and the great BET surface area of the CSNAHSs. Inductively coupled plasma mass spectrometry (ICP-MS) was also used to exactly quantify the silver content in both samples, As revealed by the measurements, the amount of silver is 4.9% (W/W) for Ag^+/CSNTs and 6.1% (W/W) for Ag^+/CSNAHSs, which coincides well with the above EDX analyses. Finally, the distribution of sliver on the Ag^+/CSNTs and Ag^+/CSNAHSs was further characterized by elememtal mapping. As shown in the elemental images (**Fig. 4e,4f)**, it is clearly seen that silver ions (yellow color, silver) were well-dispersed on the both copper silicates.

Cite this: DOI: 10.1039/c0xx00000x

www.rsc.org/xxxxxx

ARTICLE TYPE

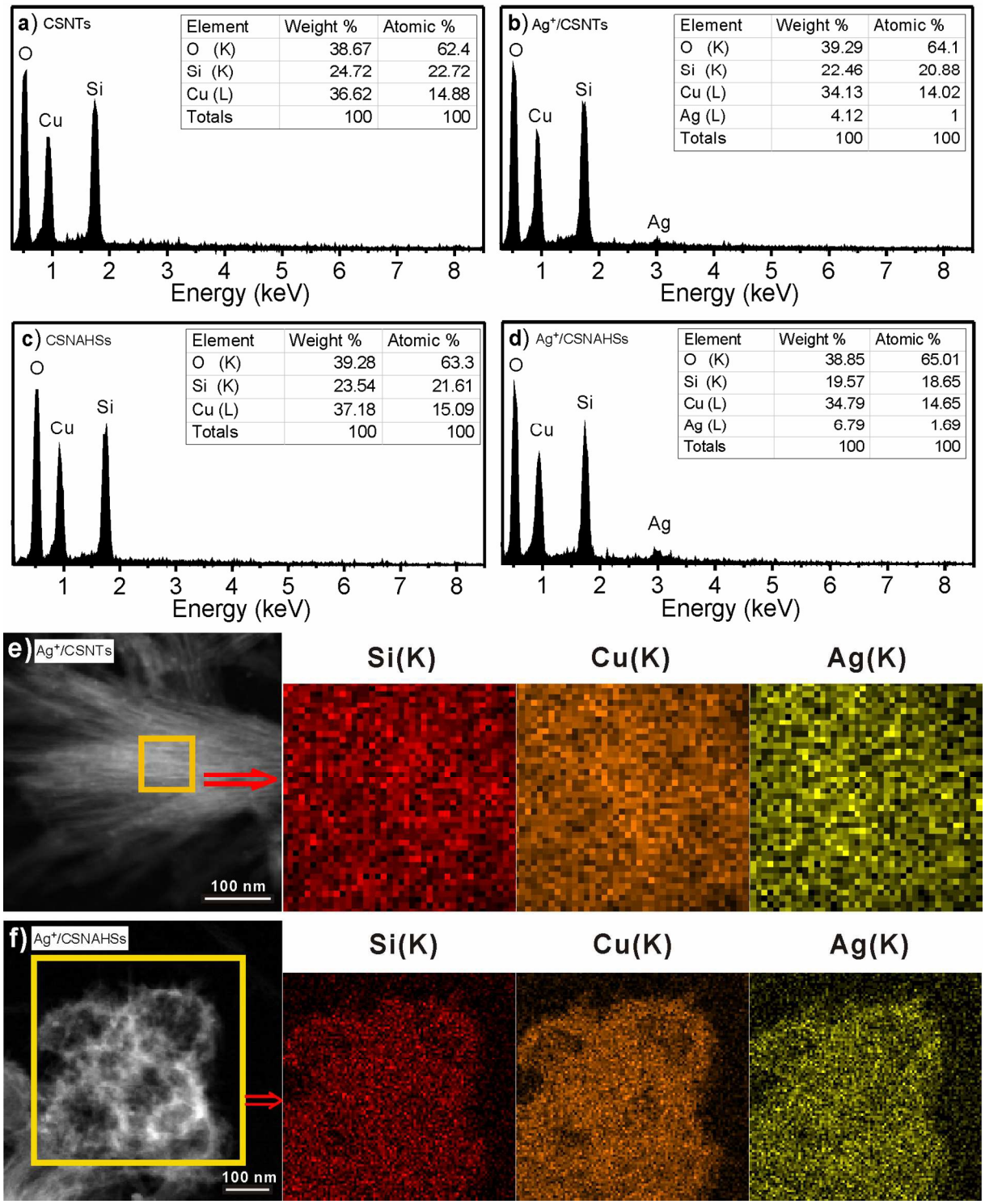

Figure 4. Energy dispersive X-ray spectra (EDX), scanning transmission electron microscopy (STEM) images and the corresponding elemental mapping images of CSNTs, Ag^+/ CSNTs, CSNAHSs and Ag^+/CSNAHSs. EDX spectra: (a) CSNTs, (b) Ag^+/CSNTs, (c) CSNAHSs and (d) Ag^+/CSNAHSs; STEM images and the corresponding elemental mapping images: (e) Ag^+/CSNTs and (f) Ag^+/CSNAHSs.

Cite this: DOI: 10.1039/c0xx00000x

www.rsc.org/xxxxxx

ARTICLE TYPE

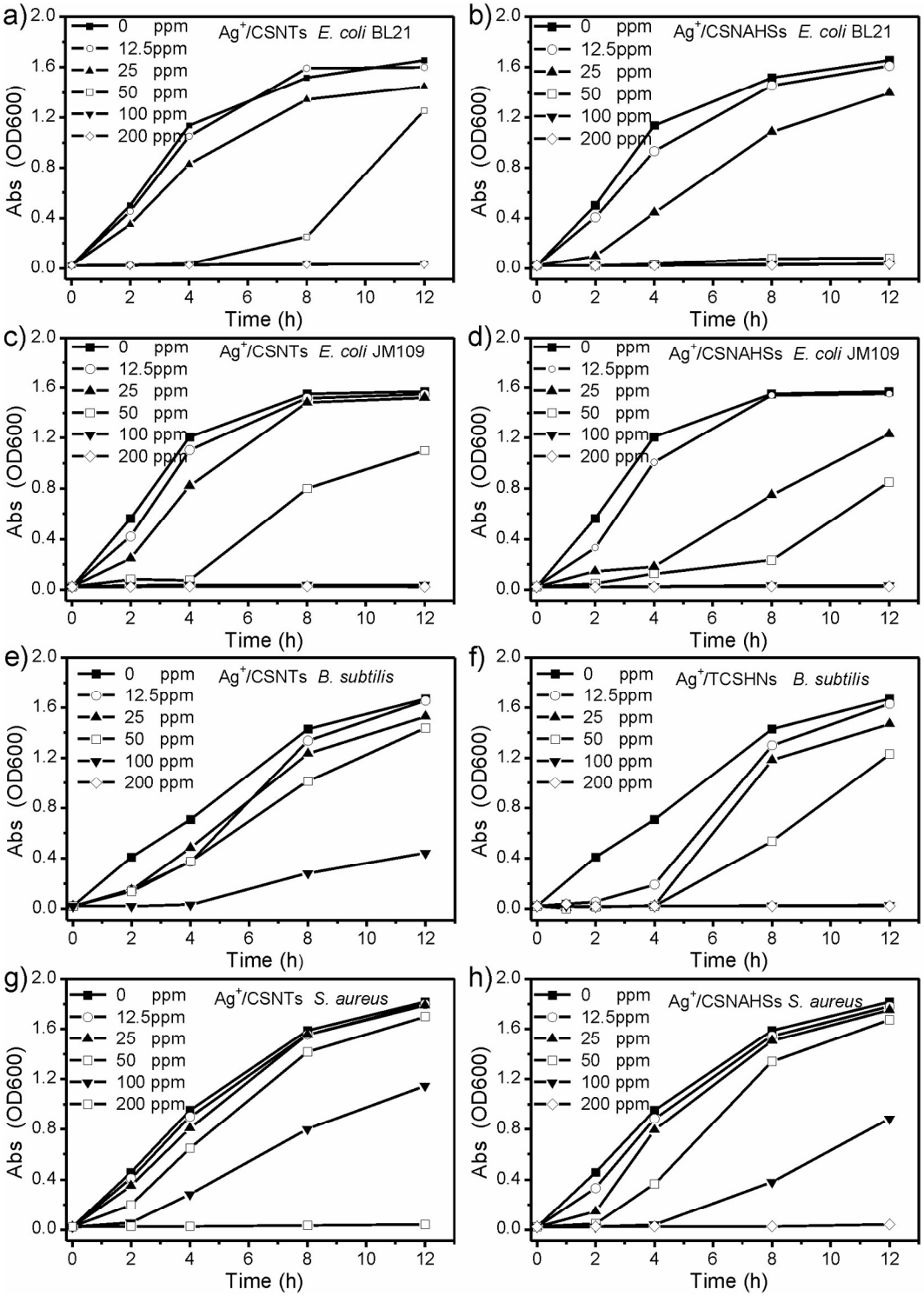

Figure 5. Bacterial growth curves in LB liquid medium inoculated with different concentrations of Ag^+/CSNTs or Ag^+/CSNAHSs. Gram-negative bacteria : (a) and (b) *E. coli* BL21, (c) and (d) *E. coli* JM109; Gram-positive bacteria: (e) and (f) *B. subtilis*, (g) and (h) *S. aureus*.

Cite this: DOI: 10.1039/c0xx00000x

www.rsc.org/xxxxxx

ARTICLE TYPE

The chemical states of Ag and Cu in both Ag^+/CSNTs and Ag^+/CSNAHSs were checked by X-ray photoelectron spectroscopy (XPS). **Fig. S1** shows the high resolution XPS spectra of Ag 3d region (**Fig. S1a**) and Cu 2p region (**Fig. S1a**). The resulting Ag 3d spectra show two main peaks centered at 368.5 eV and 374.4 eV,[47,48] suggesting that the silver in the both samples is present in the oxidized state. The XPS spectra of Cu 2p reveal that the Cu oxidation state is +2, as evidenced by the binding energy of Cu $2p_{3/2}$, Cu $2p_{1/2}$ and Cu 2p satellite at about 935.3 eV, 955.2 eV and 942-944 eV, respectively .[49,50]

The antibacterial activities of Ag^+/CSNTs and Ag^+/CSNAHSs were evaluated against *E. coli* BL21, *E. coli* JM109, *B. subtilis* and *S. aureus*. Assays were performed in silver-loaded copper silicates concentrations ranging from 12.5 to 200 μg/mL. As demonstrated in **Fig. 5**, both silver-loaded copper silicates show strong antimicrobial activities against the four types of bacterial strains. However, Ag^+/CSNAHSs display higher antibacterial activities at all tested concentrations when compared with Ag^+/CSNTs. This phenomenon may be explained by the higher silver contents in the Ag^+/CSNAHSs, as demonstrated by EDX and ICP analyses. In addition, it is also found out that the silver-loaded copper silicates show stronger antimicrobial activities against Gram-negative bacteria than Gram-positive bacteria. For instance, at 50 μg/mL concentration of Ag^+/CSNAHSs, the growth of bacterial colonies was completely prevented for *E. coli* BL21 (Gram-negative bacteria). For *S. aureus* (Gram-positive bacteria), the minimum inhibitory concentration was up to 200 μg/mL. As a controlled experiment **(Fig. S3)**, CSNTs and CSNAHSs without Ag^+ were also used, and showed a mild antibacterial effect even at high concentration.

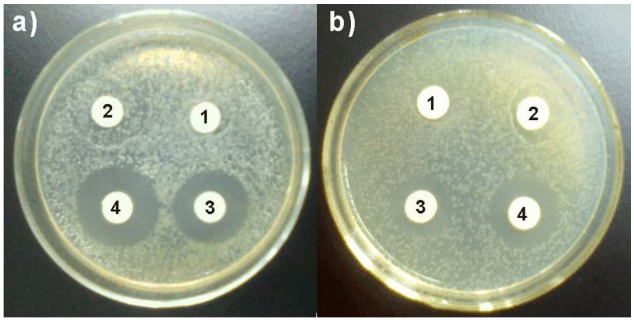

Figure 6. Inhibition zone tests of Ag^+/CSNTs, Ag^+/CSNAHSs, CSNTs and CSNAHSs against (a) *E. coli* BL21 and (b) *S. aureus*. [NO.1: CSNTs NO.2: CSNAHSs NO.3: Ag^+/CSNTs NO.4: Ag^+/CSNAHSs].

In order to clearly illustrate the different antibacterial activities between Ag^+/CSNTs and Ag^+/CSNAHSs, the inhibition zone tests were performed. The results are presented as images in **Fig. 6** and as average inhibition zone values in **Table 1**. It is obviously seen that Ag^+/CSNAHSs still show higher antibacterial activities than Ag^+/CSNTs, and the antibacterial abilities of the both silver-loaded copper silicates on *E. coli* BL21 (Gram-negative) is superior to *B. subtilis* (Gram-positive).

Table 1. The inhibition zones diameters (IZDs) for *E. coli* BL21 and *S. aureus*, based on the inhibition zone tests of **Fig. 6**.

Sample	The IZDs on strain (mm)	
	E. coli	*S. aureus*
NO.1: CSNTs	~ 9.0	~ 9.0
NO.2: CSNAHSs	~ 9.0	~ 9.0
NO.3: Ag^+/CSNTs	21.2±0.4	16.3±0.3
NO.4: Ag^+/CSNAHSs	23.8±0.2	19.2±0.2

Importantly, the CSNAHSs acting as silver ions carriers embed the antibacterial copper ions in the matrix. So it is reasonable to assume that the Ag^+/CSNAHSs possess higher antibacterial activity under simultaneous action of copper ions and silver ions, when compared with other metal ions carriers. To prove this deduction, the silver-loaded hollow mesoporous silica nanospheres (Ag^+/HMSHs)[51,52] were also synthesized to compare their antibacterial activities. As illustrated in **Fig. 7**, about 99.0 % inhibitions of the bacterial growth was observed by the Ag^+/CSNAHSs at an equivalent silver concentration of 15 μg/mL. In comparison, Ag^+/HMSHs (silver loading amount 4.0 %) and CSNAHSs exhibited a lower antibacterial activities with 33.2 % inhibitions and 13.5 % inhibitions, respectively, at the same condition. The antibacterial efficacy by the Ag^+/CSNAHSs was even higher than the sum of the antibacterial efficacy of Ag^+/HMSHs and CSNAHSs, reflecting that the synergistic effect of copper ions and silver ions on the inhibition of the bacterial growth was appeared in our bimetal antibacterial system.

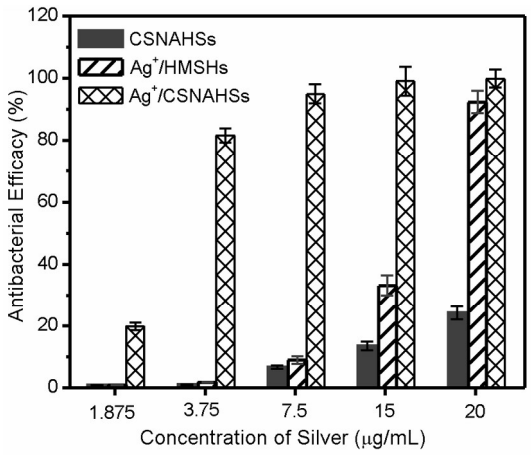

Figure 7. Antimicrobial efficacy of CSNAHSs, Ag^+/HMSHs and Ag^+/CSNAHSs, against *E. coli* BL21 in LB liquid medium.

4. Conclusions

The Cu-Ag bimetal-loaded copper silicate nanotubes and nanotube-assembled hollow nanospheres were prepared as effective antibacterial agents. The as-prepared bimetal-loaded copper silicates exhibit high antibacterial activities against *E. coli* BL21, *E. coli* JM109, *B. subtilis* and *S. aureus*. The comparative antibacterial tests reveal that Ag^+/CSNAHSs have stronger antibacterial abilities than Ag^+/CSNTs owing to their more silver contents. Moreover, we had also demonstrated that the Ag^+/CSNAHSs exhibited a synergistic effect for bacteria killing.

Acknowledgment

We thank the Natural Science Foundation of Anhui Province (1508085QB39), the National Natural Science Foundation of China (51402001), the Open Project of State Key Laboratory of Physical Chemistry of Solid Surfaces (Xiamen University) (201416), the Grants for Scientific Research of BSKY (0115027101) from Anhui Medical University, and the Program for the Outstanding Young and Middle-aged Talents (0115027102) of Anhui Medical University for the financial support.

Notes and references

[a] *College of Basic Medicine, Anhui Medical University, Hefei 230032, P.R. China; E-mail: wjfang81@163.com.*
[b] *Sate Key Laboratory of Physical Chemistry of Solid Surfaces, Xiamen University, Xiamen 361005, P.R. China.*
[c] *Center of Modern Experimental Technology, Anhui University, Hefei 230039, Anhui, P.R. China; E-mail: jzheng@ahu.edu.cn*
[#] *These authors contributed equally.*

† Electronic Supplementary Information (ESI) available. See DOI: 10.1039/b000000x/

1 D. E. De Vos, M. Dams, B. F. Sels, P. A. Jacobs, *Chem. Rev.* 2002, **102**, 3615-3640.
2 J. V. Walker, M. Morey, H. Carlsson, A. Davidson, G. D. Stucky, A. Butler, *J. Am. Chem. Soc.* 1997, **119**, 6921-6922.
3 J. Zheng, B. H. Wu, Z. Y. Jiang, Q. Kuang, X. L. Fang, Z. X. Xie, R. B. Huang, L. S. Zheng, *Chem-Asian J.* 2010, **5**, 1439-1444.
4 P. X. Liu, M. Chen, C. Chen, X. L. Fang, X. L. Chen, N. F. Zheng, *J. Mater. Chem. B* 2013, **1**, 2837-2842.
5 D. Tarn, C. E. Ashley, M. Xue, E. C. Carnes, J. I. Zink, C. J. Brinker, *Acc. Chem. Res.* 2013, **46**, 792-801.
6 D. Gu, F. Schuth, *Chem. Soc. Rev.* 2014, **43**, 313-344.
7 M. P. Mokhonoana, N. J. Coville, *Materials* 2009, **2**, 2337-2359.
8 Q. L. Fang, S. H. Xuan, W. Q. Jiang, X. L. Gong, *Adv. Funct. Mater.* 2011, **21**, 1902-1909.
9 R. D. White, D. V. Bavykin, F. C. Walsh, *J. Mater. Chem. A* 2013, **1**, 548-556.
10 D. Barreca, W. J. Blau, G. M. Croke, F. A. Deeney, F. C. Dillon, J. D. Holme s, C. Kufazvinei, M. A. Morris, T. R. Spalding, E. Tondello, *Micropor. Mesopor. Mater.* 2007, **103**, 142-149.
11 W. J. Fang, J. Yang, J. W. Gong, N. F. Zheng, *Adv. Funct. Mater.* 2012, **22**, 842-848.
12 Y. Yang, Y. A. Zhuang, Y. H. He, B. Bai, X. Wang, *Nano Res.* 2010, **3**, 581-593.
13 Y. Yang, Y. A. Zhuang, Y. H. He, B. Bai, X. Wang, *Nano Res.* 2010, **3**, 581-593.
14 A. R. Silva, H. Albuquerque, S. Borges, R. Siegel, L. Mafra, A. P. Carvalho, J. Pires, *Micropor. Mesopor. Mater.* 2012, **158**, 26-38.
15 L. F. Chen, P. J. Guo, M. H. Qiao, S. R. Yan, H. X. Li, W. Shen, H. L. Xu, K. N. Fan, *J. Catal.* 2008, **257**, 172-180.
16 G. Prieto, J. Zecevic, H. Friedrich, K. P. de Jong, P. E. de Jongh, *Nat. Mater.* 2013, **12**, 34-39.
17 J. J. Xue, X. Q. Wang, G. S. Qi, J. Wang, M. Q. Shen, W. Li, *J. Catal.* 2013, **297**, 56-64.
18 K. L. Deutsch, B. H. Shanks, *J. Catal.* 2012, **285**, 235-241.
19 T. Toupance, M. Kermarec, J. F. Lambert, C. Louis, *J. Phys. Chem. B* 2002, **106**, 2277-2286.
20 G. Borkow, J. Gabbay, *Curr. Med. Chem.* 2005, **12**, 2163-2175.
21 G. Grass, C. Rensing, M. Solioz, *Appl. Environ. Microbiol.* 2011, **77**, 1541-1547.
22 M. J. Hajipour, K. M. Fromm, A. A. Ashkarran, D. J. de Aberasturi, I. R. de Larramendi, T. Rojo, V. Serpooshan, W. J. Parak, M. Mahmoudi, *Trends Biotechnol.* 2012, **30**, 499-511.
23 S. Mallick, S. Sharma, M. Banerjee, S. S. Ghosh, A. Chattopadhyay, A. Paul, *ACS Appl. Mater. Inter.* 2012, **4**, 1313-1323.
24 H. R. Yue, Y. J. Zhao, S. Zhao, B. Wang, X. B. Ma, J. L. Gong, *Nat. Commun.* 2013, **4**, 2339-2342.
25 X. Wang, J. Zhuang, J. Chen, K. B. Zhou, Y. D. Li, *Angew. Chem. Int. Ed.* 2004, **43**, 2017-2020.
26 Y. Q. Wang, G. Z. Wang, H. Q. Wang, W. P. Cai, L. D. Zhang, *Chem. Commun.* 2008, **48**, 6555-6557.
27 J. Qu, W. Li, C. Y. Cao, X. J. Yin, L. Zhao, J. Bai, Z. Qin, W. G. *J. Mater. Chem.* 2012, **22**, 17222-17226.
28 C. R. Martin, P. Kohli, *Nat. Rev. Drug Discov.* 2003, **2**, 29-37.
29 C. C. Chen, Y. C. Liu, C. H. Wu, C. C. Yeh, M. T. Su, Y. C. Wu, *Adv. Mater.* 2005, **17**, 404-407.
30 C. H. Wu, C. Cao, J. H. Kim, C. H. Hsu, H. J. Wanebo, W. D. Bowen, J. Xu, J. Marshall, *Nano Lett.* 2012, **12**, 5475-5480.
31 W. Feng, P. Ji, *Biotechnol Adv.* 2011, **29**, 889-895.
32 P. Khare, A. Sharma, N. Verma, *J. Colloid Interf. Sci.* 2014, **418**, 216-224.
33 K. T. Chen,; D. T. Ray, Y. H. Peng, Y. C. Hsu, *Curr.. Appl. Phys.* 2013, **13**, 1496-1501.
34 I. Slamborova, V. Zajicova, J. Karpiskova, P. Exnar, I. Stibor, *Mat. Sci. Eng. C-Mater.* 2013, **33**, 265-273.
35 M. Zhang, P. Wang, H. Sun, Z. Wang, *ACS Appl. Mater. Inter.* 2014, **6**, 22108-2215.
36 S. Mallick, P. Sanpui, S. S. Ghosh, A. Chattopadhyay, A. Paul, *Rsc Adv* 2015, **5**, 12268-12276.
37 S. Demirci, Z. Ustaoglu, G. A. Yilmazer, F. Sahin, N. Bac, *Appl. Biochem. Biotech.* 2014, **172**, 1652-1662.
38 B. Q. Jia, Y. Mei, L. Cheng, J. P. Zhou, L. N. Zhang, *ACS Appl. Mater. Inter.* 2012, **4**, 2897-2902.
39 T. A. Dankovich, J. A. Smith, *Water Res.* 2014, **63**, 245-251.
40 E. A. Abou Neel, I. Ahmed, J. Pratten, S. N. Nazhat, J. C. Knowles, *Biomaterials* 2005, **26**, 2247-2254.
41 S. Chernousova, M. Epple, *Angew. Chem. Int. Ed.* 2013, **52**, 1636-1653.
42 W. J. Fang, J. Zheng, C. Chen, H. B. Zhang, Y. X. Lu, L. Ma, G. J. Chen, O *J. Magn. Magn. Mater.* 2014, **357**, 1-6.
43 C. Carolina, B. J. Carlos, B. M. L. Zapata, Z. J. Manuel, *Micropor. Mesopor. Mater.* 2014, **188**, 118-125.
44 A. M. Fonseca, I. C. Neves, *Micropor. Mesopor. Mater.* 2013, **181**, 83-87.
45 Y. Tian, J. Qi, ,W. Zhang, Q. Cai, X. Jiang, *ACS Appl. Mater. Inter.* 2014, **6**, 12038-12045.
46 Y. Zhou, Y. Deng, P. He, F. Dong, Y. Xia, Y. He, *Rsc Adv* 2014, **4**, 5283-5288.
47 W. J. Fang, L. Ma, J. Zheng, C. Chen, *J. Mater. Sci.* 2014, **49**, 3407-3413.
48 V. K. Kaushik, *J. Electron Spectrosc. Relat. Phenom.* 1991, **56**, 273-277.
49 J. L. Gong, H. R. Yue, Y. J. Zhao, S. Zhao, L. Zhao, J. Lv, S. P. Wang, X. B. Ma, *J. Am. Chem. Soc.* 2012, **134**, 13922-13925.
50 Y. H. Kim, D. K. Lee, H. G. Cha, C. W. Kim, Y. C. Kang, Y. S. Kang, *J. Phys. Chem. B* 2006, **110**, 24923-24928.
51 W. J. Fang, S. H. Tang, P. X. Liu, X. L. Fang, J. W. Gong, N. F. Zheng, *Small* 2012, **8**, 3816-3822.
52 X. L. Fang, X. J. Zhao, W. J. Fang, C. Chen, N. F. Zheng, *Nanoscale* 2013, **5**, 2205-2218.